Inferring the Interfacial Reactivity of Gold Nanoparticles by Surface Plasmon Resonance Measurements

Mélanie Romain, Phoölan Roman, Lucien Saviot, Nadine Millot, Wilfrid Boireau

Inferring the interfacial reactivity of gold nanoparticles from Surface Plasmon Resonance measurements

*Mélanie Romain[1], Phoölan Roman[2], Lucien Saviot[1], Nadine Millot[*3] and Wilfrid Boireau[*2]*

[1]Laboratoire Interdisciplinaire Carnot de Bourgogne, UMR 6303 CNRS/Université Bourgogne Franche-Comté, 9 Avenue Alain Savary, BP 47870, Dijon, 21078 France

[2]Université de Franche-Comté, CNRS, institut Femto-ST, F-25030 Besançon, France

[3]Laboratoire Interdisciplinaire Carnot de Bourgogne, UMR 6303 CNRS/Université de Bourgogne, BP 47870, Dijon, 21078 France

* Nadine.Millot@u-bourgogne.fr ; wilfrid.boireau@femto-st.fr

Keywords: gold nanoparticles; surface plasmon resonance; functionalization; thiols; reactivity; SAM; self-assembled monolayer

Abstract:

Gold nanoparticles (GNPs) require a functionalization step in most cases to be suitable for applications. Optimizing this step in order to maintain both the stability and the plasmonic properties of the GNPs is a demanding process. Indeed, multiple analyses are required to get sufficient information on the grafting rate and the stability of the obtained suspension, leading to material and time waste. In this study, we propose to investigate the ligand reactivity on a gold surface with surface plasmon resonance (SPR) measurements as a way to simulate the reactivity in GNPs suspensions. We consider two thiolated ligands in this work: thioglycolic acid (TA) and 6-mercaptohexanoic acid (MHA). These thiols are grafted using different conditions on GNPs (monitored by optical absorption) and on a gold surface (monitored by SPR) and the grafting efficiency and stability are compared. The same conclusions are reached in both cases regarding the best protocol to implement, namely that the thiol molecules should be introduced in a water solution at a low concentration. This demonstrates the suitability of SPR to predict the reactivity onto GNPs surface.

Introduction

Gold Nanoparticles (GNPs) have been used for centuries, until being considered as essential in many fields of nanotechnology due to their numerous applications [1-2]. Indeed, gold has unique properties namely a high atomic number, high chemical stability and biocompatibility, ease of NPs synthesis and modulation of size and shape, facile attachment of variety of molecules and the resulting plasmonic properties. All those distinctive characteristics have made GNPs attractive for many applications such as sensing [3], catalysis [4], enhanced optoelectronics [5], photovoltaics [6], plasmonics [7], and bioapplications [2, 8] (bioimaging [9], drug delivery [10], radiosensitizing [11-12] and photothermal therapy[13]). To control the final properties of GNPs, one needs to control the synthesis parameters and choose adapted surface functionalization. This critical step ensures the colloidal stability and desired reactivity if applicable [14-16]. Different routes exist for the synthesis of colloidal GNPs. One of the most used is the Turkevich-Frens method where hot chloroauric acid ($HAuCl_4$) is reduced by sodium citrate which also acts as a stabilizer [17-19], stabilization occurs electrostatically which facilitates subsequent functionalization by ligand exchange thanks to the weak bonding of citrates onto gold surfaces [20-22]. The high affinity of thiols for gold makes thiol derivatives among the most convenient/adapted molecules for such reactions. However, the electrostatic repulsions between the nanoparticles may disappear after ligand exchange, which can destabilize the suspension leading to aggregation [15, 23-25]. The choice of the ligand and the study of its replacement protocol and kinetics is therefore crucial.

Different methods are available to study the final thiol molecules layer such as thermogravimetry [26-27], X-ray photoelectron spectroscopy [28], electron microscopy [29]. Another non-destructive very efficient way is the monitoring of the localized surface plasmon resonance (LSPR) of the GNPs by UV-visible spectroscopy [1, 30-31]. For noble metal nanoparticles such as GNPs, the optical properties are due to coherent oscillations of conduction band electrons in the NPs in resonance with an electromagnetic radiation (LSPR) [32]. LSPR is easily analyzable for spherical GNPs by UV-Visible spectroscopy. It manifests as bands generally near 510-540 nm depending on the size of the NPs and the refractive index of the surrounding medium [33]. As a result, this resonance may shift after molecular grafting at the surface [34]. A closely related optical property (surface plasmon polariton) is also used in gold films for another type of plasmonic biosensor known as surface plasmon resonance (SPR) [35-37]. SPR is a very sensitive technique to study biomolecular interactions by measuring changes over time in the refractive index of a complex media surrounding a metal-based film which is most of time made of gold. Modifications are monitored *via* the change of the angle at which the plasmonic properties are optimum (*i.e.* at the minimum of reflectivity, of the light source that is focused on the metal film and reflected to a detector). SPR is therefore a label-free technique widely used to study the interactions between two macromolecules, one being immobilized on the sensor surface and the other one being in the surrounding medium contained into a microfluidic system [38]. This method provides not only information on the affinity between the molecules through the binding strength, but also on the kinetics of their association-dissociation with on and off rates [39-41].

Although SPR is a gold standard method for the analysis of biomolecular interactions, it is however generally not used to study interactions of small molecules (molecular weight below 150 Da), and not routinely employed to monitor the adsorption processes onto bare gold surfaces. Kinetics of adsorption of small thiolated compounds has been previously obtained by using SPR on a few molecules such as L-Cysteine, 1-hexane thiol and 11-mercaptoundecanoic acid [42-44]. For larger molecules, their non-solubility in aqueous phases generally prevents conducting such experiments. To the best of our knowledge, there is no previous report of using SPR as a tool to study interfacial reactivity in a system where the gold surface chip mimics the gold nanoparticle surface. It is known that the ligand exchange by thiol derivatives on GNPs surfaces are dictated by the curvature. Therefore, the kinetic and thermodynamic profiles can be different from the ones observed on flat gold surfaces [45]. However, the roughness of the surface of the gold layer constituting the SPR chip makes it comparable to a continuous monolayer of gold grains exposing the top part of GNPs of about 30 nm in diameter [46]. In this way, SPR allows an easy screening of the trends in reactivity and therefore on the best conditions to employ for the grafting of thiolated molecules on the gold surface. This faster method can save time and materials compared to tests carried out on GNPs batches. It also brings qualitative information on the formation kinetics of self-assembled monolayers (SAMs), and quantitative information on the amount of grafted molecules.

In the present article, we study the interaction of two molecules, namely thioglycolic acid (TA) and 6-mercaptohexanoic acid (MHA), with the gold chip surface for different conditions of concentration and solvent. The results are then compared with the behavior of GNPs suspensions functionalized under the same conditions.

Materials and Methods

Materials: Tetrachloroauric acid trihydrate ($HAuCl_4.3H_2O$, 99.99%) was purchased from ThermoFischer Scientific. Tri-sodium citrate trihydrate ($C_6H_5Na_3O_7 \cdot 2H_2O$, >99% FG), thioglycolic acid (TA, $HSCH_2COOH$, >99%), 6-mercaptohexanoic acid (MHA, $HS(CH_2)_5COOH$, 90%) and Octyl glucopyranoside (OG) were purchased from Sigma Aldrich. Ethanol absolute was purchased from VWR. All aqueous solutions were prepared with ultrapure water with a resistivity >18.2 MΩ.

GNPs synthesis: GNPs of 16 nm were synthetized using the Turkevich-Frens method. All glassware was pre-washed with aqua regia. 100 mL of a 0.28 mM $HAuCl_4 \cdot 3H_2O$ solution was heated at 100°C in a 250 mL two-necked round-bottom flask upon agitation under reflux. Then 10 mL of a 0.030 M sodium citrate tribasic dihydrate solution was quickly added to the gold solution. The temperature was maintained for 40 min, and then stopped to let the mixture cool down to room temperature.

GNPs functionalization: Mercapto-acids (MA) (see structure in Figure S1) were grafted to the GNPs surface by ligand exchange. In a glass flask with stirrer, a 25.4 mM MA solution was injected into the as-prepared GNPs suspension with an Au:S molar ratio equal to 1:0.1. We choose this value slightly above the calculated ratio (0.04 assuming a 5.1 molecules/nm^2) in order to favor the reaction despite the small concentration of GNPs.

The mixture was stirred at 400 rpm at 25°C in the dark for 1 h before being washed twice by centrifugation during 10 min at 5000 G and resuspended in ultrapure water. One centrifugation is enough to remove excess MA and citrates when controlling supernatant conductivity only. A second one was used as a precaution before Raman measurements. Additional centrifugations tend to destabilize and decrease the suspension concentration.

Functionalization was also tested with a higher MA solution concentration of 2.5 mM and with a 25.4 mM MA solution but with a 10% (v/v) EtOH as a solvent, in which case only one centrifugation was achieved.

SPR experiments: All experiments were performed with a Biacore 3000 setup from GE Healthcare (Uppsala, Sweden) at 25°C. Sensor chips were gold deposited glass slides fabricated in clean room. It is composed of four channels of 1.2 mm² surface. To mimic the conditions of in the GNPs suspension grafting, the gold chip surface was conditioned with sodium citrate by using a 2.7 mM sodium citrate solution as running buffer. 200 µL of MA solutions were then injected at 4 mL/min through four different channels to compare different conditions summarized in Table 1:

Test	[SH]	Solvent
1	25.4 µM	2.7 mM citrate in H_2O
2	2.5 mM	2.7 mM citrate in H_2O
3	25.4 µM	2.7 mM citrate in H_2O + EtOH
4	1.3 µM	2.7 mM citrate in H_2O

Table 1. Experimental conditions tested for SPR experiments with variations in mercapto-acids concentration and solvent.

The thiol concentration used for GNPs functionalization is 25.4 µM. The 2.5 mM concentration was used to obtain a very large excess. Conditions are still slightly different if the same concentration is used on nanoparticles and in SPR. Indeed, the ratio of the amount of thiol over the amount of interface slightly differs. Indeed, spherical GNPs of 16 nm have a surface of 804 nm^2 and a concentration of 1.2×10^{12} NPs/mL. With the functionalization ratio used of Au:S=1:0.1 (molar), it introduces 15.7 SH/nm^2. The gold surface of a channel within the SPR microfluidic chip is 1.2 mm^2 [47]. To get the same amount of thiol available for the gold surface, an injection of 20 µL should have a concentration of 1.3 µM. This concentration is thus tested as a comparison in the SPR system.

Finally, ethanol is often used for the solubilization of alkanethiols whose terminal groups are the only hydrophilic ones. The aliphatic chain is more soluble in EtOH which helps limiting disulfide bond formation. But the use of EtOH in that case of functionalization leads to additional attention upon washing, and its necessity to solubilize such short chains as the ones of TA and MHA is debatable. Thus, a grafting of MA in 10% EtOH is tested here to assess its effect on the efficiency of functionalization.

Signal balance in response units (RU) is given after two 25 µL octyl glucopyranoside (OG) injections at 50 µL/min for washing.

Dynamic light scattering (DLS): Hydrodynamic diameters were measured with a Malvern Nano ZS instrument (Worcestershire, UK) supplied by DTS Nano V7.11 software. 1 mL of as prepared GNPs suspensions were poured in disposable cuvettes. Then 3 measurements with

Refractive Index = 0.200 and Absorption = 3.320 are recorded. The intensity distributions are obtained from the mean value of these 3 measurements.

UV-Visible spectroscopy: The absorbance of the as-prepared or functionalized GNPs suspensions were measured with a Shimadzu UV-2550 spectrophotometer (Tokyo, Japan). 1.5 mL suspension were poured in disposable cuvettes. All the spectra were recorded from 400 to 800 nm at 25°C. The baseline was measured with deionized water. Spectrometer resolution is 0.1 nm.

Transmission electron microscopy (TEM): The morphology and size of the GNPs were analyzed by transmission electron microscopy with a Hitachi HT7800 setup with an acceleration voltage of 100 kV. The samples were prepared on carbon-coated copper grids by evaporation of the suspension after soaking of the grid. The mean particle size was calculated from measurements of 300 GNPs analyzed with the Image J software.

Raman spectroscopy: Drops of the suspensions were deposited onto glass microscope slides. The measurements were obtained with a Renishaw inVia microspectrometer using the 785 nm excitation line of a diode laser and an x50 microscope objective. Care was taken to keep the laser power low enough to prevent heating the sample.

Results and Discussion

Synthesis and functionalization of the gold nanoparticles

DLS, TEM image and a picture of the pink suspension of the obtained GNPs are presented in Figure 1. They show a monodisperse population of mainly spherical NPs (some are faceted), with a mean diameter of 15.4 ± 1.5 nm as measured by TEM and 14.3 ± 3.8 nm as obtained from the DLS size distribution by number (Figure S2 for TEM size distribution). The maximum in the UV-visible spectrum correspond to the LSPR band. It enables to determine the size of the obtained

GNPs. We obtain 14.7 ± 2.6 nm using Haiss *et. al* formula [33]. The values obtained with the three measurements agree quite well and show that the NPs are well-dispersed and almost spherical.

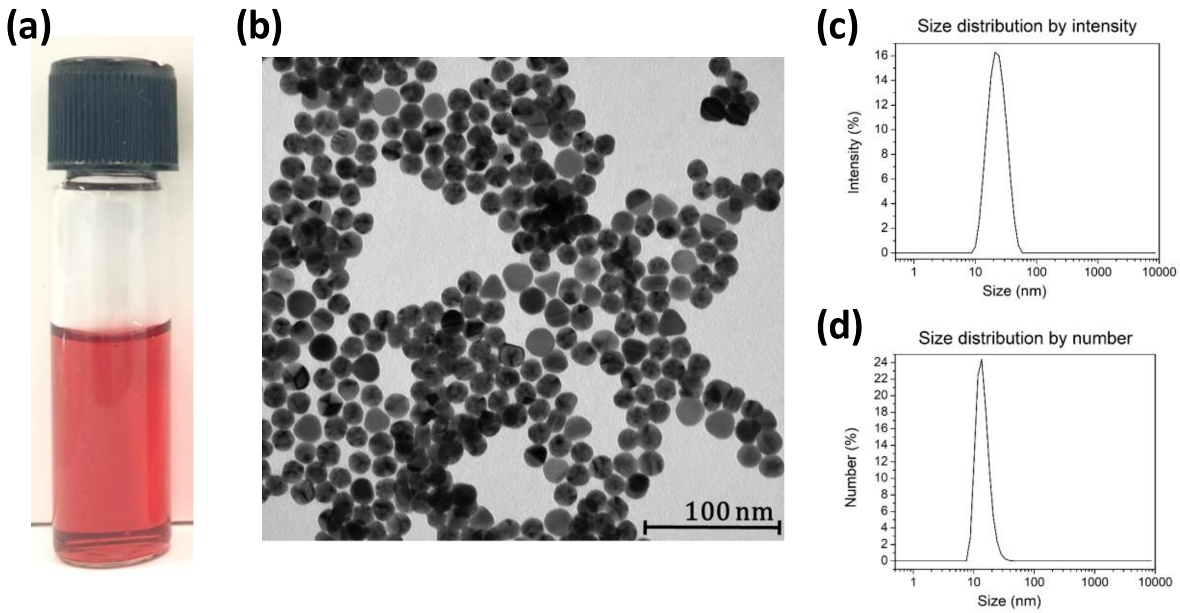

Figure 1. (a) Photograph of the GNPs suspension (b) TEM picture of synthetized GNPs (c) Size distribution of the suspension obtained by DLS by intensity (d) Size distribution of the suspension obtained by DLS by number

The functionalization of the GNPs suspension was achieved by mixing it with TA or MHA for an hour to leave some time for ligand exchange. The solution was then washed by centrifugation and redispersed to remove the excess MA and sodium citrate. After washing, the suspension remains stable as shown by the UV-Vis spectra in Figure 2 where the LSPR peak shape remains for grafted samples.

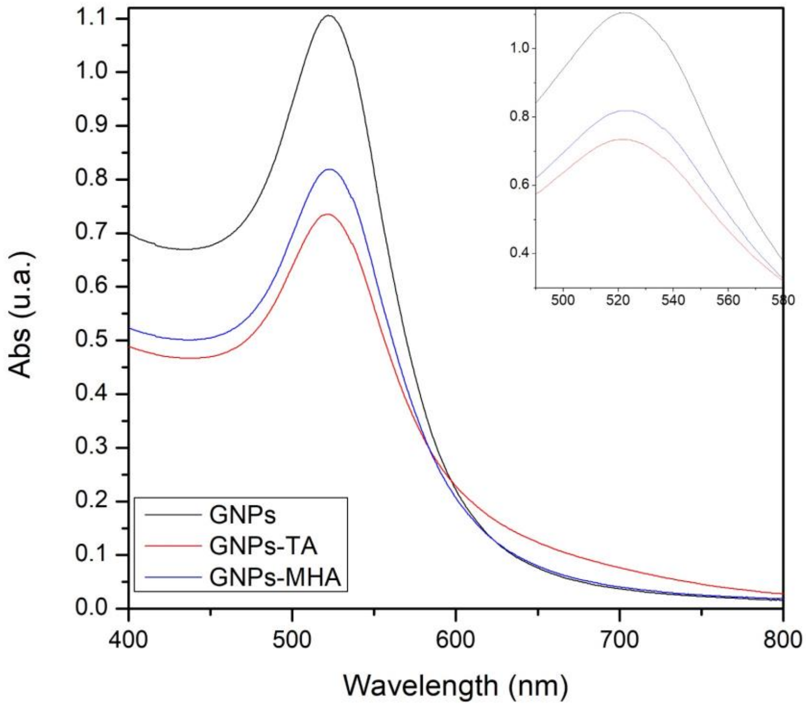

Figure 2. UV-visible spectra of the GNPs suspensions and GNPs suspension functionalized with MA after washing. The inset shows a zoom-in of the maximum LSPR peak

The spectra also show a small shift of the peak between naked GNPs ($LSPR_{max}$ = 522nm), and GNPs grafted with TA ($LSPR_{max}$ = 522.5nm) or with MHA ($LSPR_{max}$ = 523nm). This LSPR shift originates from the variation of the refractive index around the GNPs resulting from the grafting of the different molecules.

To confirm the presence of the MA molecules, the samples were investigated using Raman spectroscopy. The resulting SERS spectra are represented in Figure 3. Very different vibrational modes are observed for the as-prepared and functionalized GNPs.

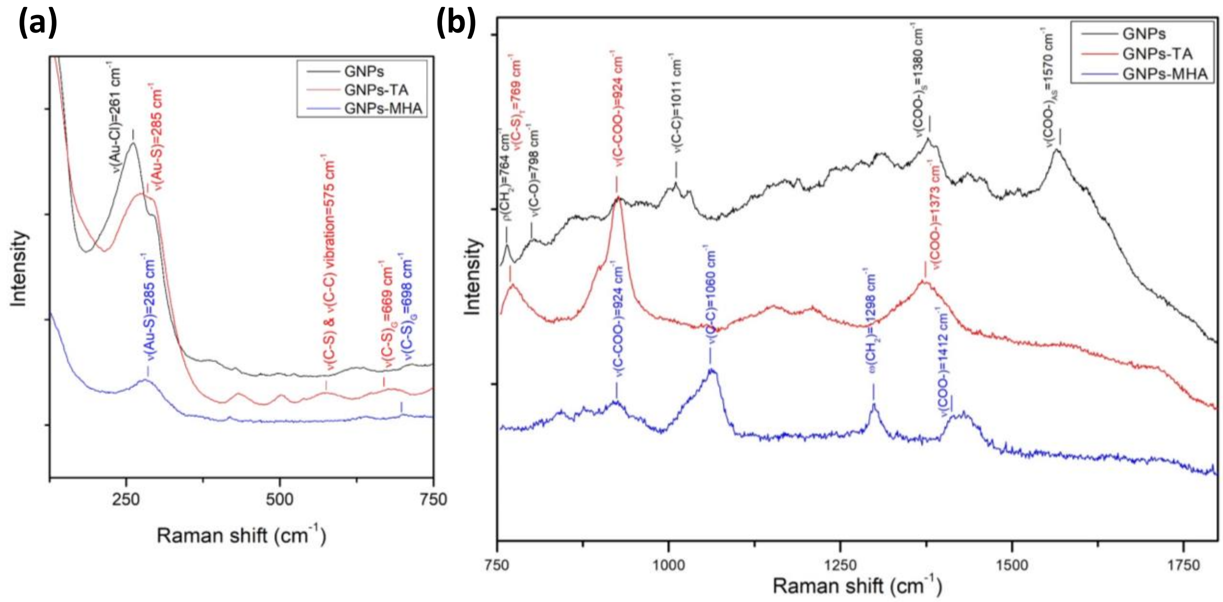

Figure 3. Raman spectra of the GNPs without modifications and after functionalization with MA and washing

Reproducible data were obtained during the analysis. The Raman intensity is lower for GNPs-MHA. GNPs stabilized with sodium citrate in excess present bands at 798 and 1011 cm^{-1} relative to stretching of C-O and C-C bonding respectively that was described in the literature [48]. Stretching bands of symmetric and antisymmetric COO^- bonding at 1380 and 1570 cm^{-1} are present due to the presence of free molecules in the sample.

The band corresponding to the stretching of the C-S bonds is visible at 769 cm^{-1} for the samples grafted with TA and with a weak intensity for ν(C-S) G conformers on both GNPs-MA samples at 669 cm^{-1} and 698 cm^{-1}, but not on the initial citrate-capped sample. This indicates the presence of sulfur atoms and therefore MA molecules around the grafted sample [49-50]. MA grafting is also confirmed by the stretching of Au-Cl bonding for citrate capped GNPs at 261 cm^{-1} that is shifted to 285 cm^{-1} for GNPs-MA for ν(Au-S). The band at 575 cm^{-1} for GNPs-TA was previously described as a complex vibration between ν(C-S) and ν(C-C) [50]. A band for the stretching of C-C bonds arises at 1060 cm^{-1} on GNPs-MHA sample due to the longer alkyl chain, confirming the presence of the molecule around GNPs [51]. The functionalized suspensions are stable as confirmed by the UV-visible spectra after 1 month (Figure S3).

With a well-established protocol, it is possible to functionalize GNPs with mercapto-acids. However, complementary characterizations such as DLS, UV-visible or Raman spectroscopies are required to check the efficiency of the grafting procedure and the resulting stability.

Evaluation of the grafting conditions by SPR

In the following, we propose to monitor the variation of the surface plasmon resonance during *in situ* functionalization of the gold surface and to compare with the previous batch approach where GNPs were functionalized in suspension by different MA, as represented in Figure 4.

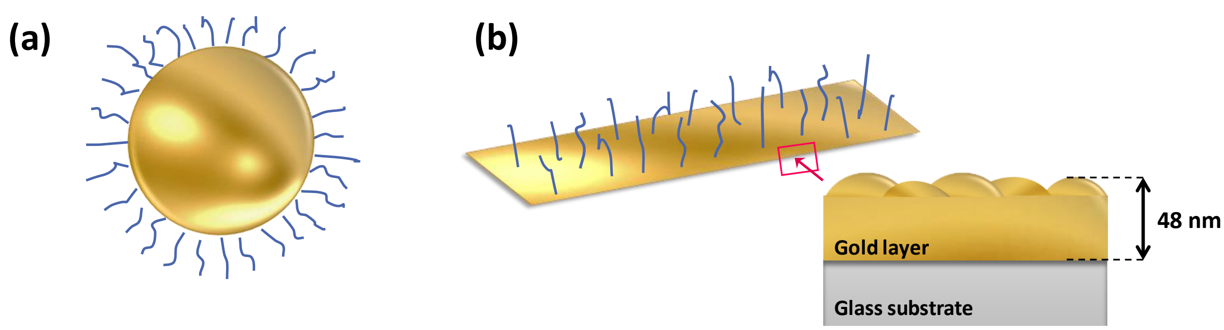

Figure 4. Schematic illustration of the compared systems with (a) a GNP surrounded by the grafted MA and (b) a layer of MA on a gold surface in the case of the SPR chip

MA solutions are injected in the SPR system after the surface was passivated with sodium citrate used as running buffer to imitate the batch system. Figure 5 shows the data obtained when injecting TA in flowchannel 1 (FC) and MHA in FC2 at 25.4 µM in the system. The results are summarized in Table 2.

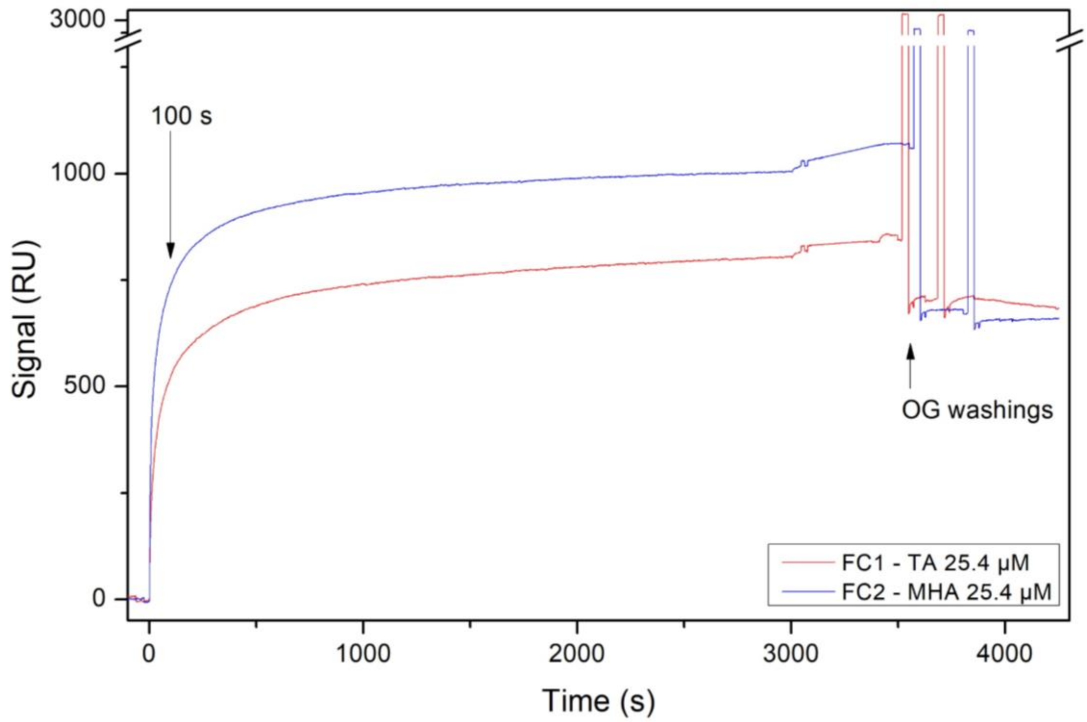

Figure 5. Sensorgrams obtained in SPR of self-assembly of MA onto gold surface by injection at 25.4 µM. (OG: octylglucopyranoside)

The injection starts at t = 0. The signal of all FCs increases quickly due to a fast interaction of the MA with the gold surface. This interaction induces just like for the batch system a change in the local environment of the plasmonic structure due to the grafting of the MA molecules and the resulting local refractive index changes. Thus, the response level witnesses the kinetics of the interaction between MA and gold. Figure 5 shows an immediate drastic increase of the signal in barely 100 s (where 65% and 73% of the signal are reached for FC1 and FC2 respectively), followed by a much slower increase during the additional 2900 s of injection. This can be interpreted as an almost immediate reaction between MA and the gold surface with instant thiol grafting onto most of the gold surface, followed by additional grafting on the remaining surface and a re-organization of the MA layer. When the injection is stopped at t = 3000 s, the system goes back to "running buffer" flow and the signal balance represents the gain of molecular mass on the FC surface based on empirical and/or theoretical correlations [52-53]. A slight positive signal drift is observed indicating the MA layer re-organization, and probably the presence of additional mass to the MA layer due to adsorption of excess MA molecules embedded onto the grafted layer. To remove this excessive molecular mass, two washings are carried out by injecting OG, a non-ionic surfactant, at a concentration superior to its critical micelle concentration (CMC) to flush out non-grafted molecules. These injections start at t = 3515 s for FC1 and t = 3570 s for FC2 and result in the sudden signal increase for 30 s. After washing, the signal is stable but the remaining signal balance is decreased compared to the one after MA injection. This supports the necessity of washing the excessive adsorbed molecules. The signal balance is 708 RU for TA in FC1 and 657 RU for MHA in FC2. Surprisingly, the signal balance is higher for TA despite its lower molar mass than MHA (M=92 $g.mol^{-1}$ for TA and M=148 $g.mol^{-1}$ for MHA). A monolayer of TA should therefore be less heavy and lead to a smaller signal increase than a monolayer of MHA. We assign this discrepancy to either the formation of multiple TA layer or a non-saturated MHA layer with some MHA molecules lying on the surface and preventing the grafting of other molecules.

To assess the grafting efficiency, we estimate the thiol grafting density with formula (1).

$$1 \text{ RU} = 1 \times 10^{-3} \text{ ng/mm}^2 \qquad (1)$$ [47]

We obtain 4.6 molecules/nm^2 for TA and 2.6 molecules/nm^2 for MHA. These are close to a dense SAMs of thiol which have a density of 5.1 molecules/nm^2 [54] for TA, and a lower value for MHA. This value was determined for alkanethiols with no potential steric repulsion at the external layer part which explains the lower value obtained for TA. The MHA layer does not seem to be closely packed, yet it is quite dense.

Other experiments were run to define the best conditions for MA grafting on gold. For an unsaturated MA layer, it may be interesting to increase concentration to favor the grafting reaction. The same experiment was conducted with a higher MA concentration of 2.5 mM. The results are presented in Figure 6. The same type of kinetic profile is obtained.

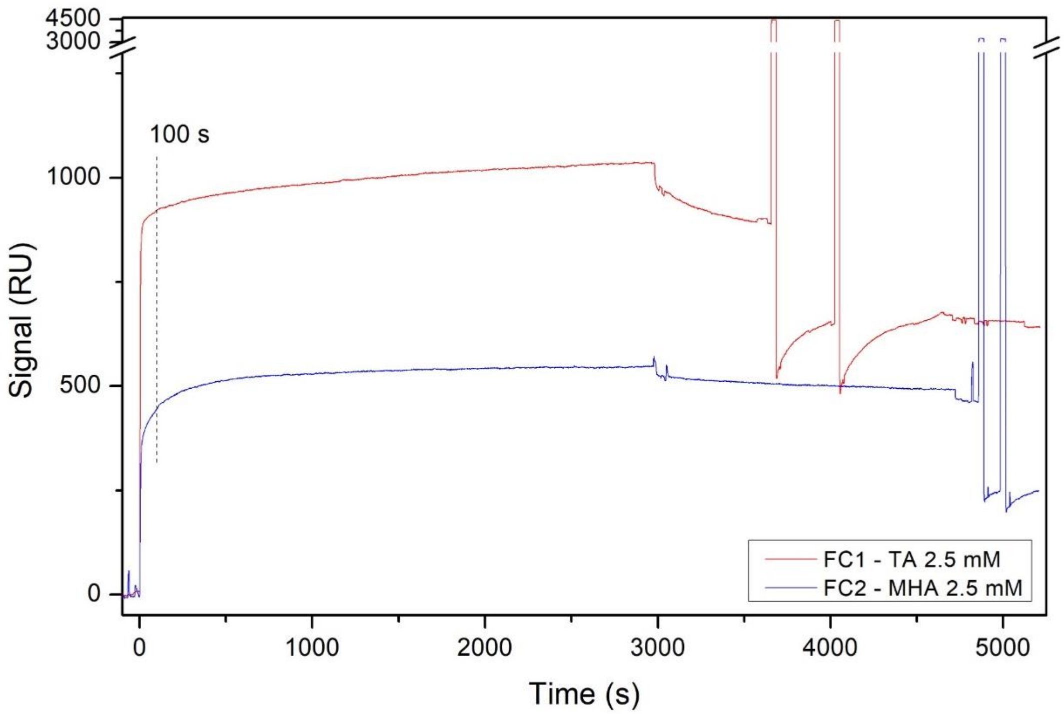

Figure 6. Sensorgrams obtained in SPR of self-assembly of MA onto gold surface by injection at 2.5 mM

As before, a drastic increase of the signal occurs instantly after the start of the MA injection at t=0s, followed by a much slower signal increase for the rest of the injection. At a higher concentration, the grafting is much faster for the two different MA. After 100s, 89% of the signal increase is reached for TA and 91% for MHA. After the injection, a slight drop of the signal indicates a small contribution from the different refractive index of the concentrated solution that was injected and a light dissociation for TA. However, the signal decrease is more pronounced after the two OG washings. Then they increase slowly especially for TA, so the systems are clearly not stable. The signal level drop is assigned to the removal of multiple layers whose formation is favored at high concentration, followed by a signal increase due to a layer re-organization after this violent molecular stall. Performing surface assembling with a high concentration of thiolated molecules induces disorganized SAMs, that can be overcome by washing steps. Also, the signal balance for the MA grafting 100 s after the second OG washing is lower than at the previous lower concentration. The signal balance is 576 RU for TA at 2.5 mM in FC1 and only 237 RU for MHA in FC2 which indicates a lower MA grafting efficiency, especially for MHA. At such a high concentration in water, disulfide bridges can form between two thiol groups, preventing them to bind with the gold surface or at least slowing down the process, which could explain such low grafting levels. Treating the solution with reducing agents such as DTT may be an interesting solution to avoid it.

Ethanol being less polar than water, adding ethanol as a solvent may help prevent the formation of disulfide bridges. In addition, ethanol also is the most widely used solvent to prepare SAMs. [55] Indeed, ethanol is inexpensive, available in high purity, has low toxicity and solvates many thiolates. It is also used for thiol functionalization of GNPs in batch. We ran the same experiment in SPR with an injection of MA at 25.4 µM again but in EtOH:H_2O = 1:10 (v/v). The results are shown in Figure S4. They show intense peaks from 1160 s for TA and 1310 s for MHA, which are due to degassing of the ethanol in the SPR device which leads to an alteration of the baseline. To avoid it, repeated short injections with identical cumulative time were carried out instead of one long injection to obtain the final signal balance.

The signal increase (Figure S4 for resulting sensorgram in SPR) at the start of the injection is now higher due to the change of refractive index in the presence of ethanol. After this rapid increase, a plateau of around 100s is observed. Then the signal increases slightly as in previous experiments. The signal balance is 679 RU for TA and 629 for MHA. Even if these values are quite high, they are lower than the ones obtained with only water as a solvent. Thus, there is no real advantage in using EtOH in this functionalization because the grafting amount doesn't increase significantly.

We explain these results by the chemical reduction of gold atoms upon immersion with ethanol which ends up weakening the thiol-gold contacts. [56] It can also modify the pH which can influence the formation of semi-covalent Au-S bonds.

Finally, a comparison was made with an even lower concentration of MA of 1.3 µM. Results in Figure S5 show a slower initial kinetics, but still a relatively small time is necessary for the signal to reach a plateau and so for the thiol grafting. The signal balance after washings is quite similar for TA and MHA, yet slightly lower than for the other concentration. This indicates that a too low concentration leads to low grafting rates. This also implies that the choice of concentration in order to introduce a similar thiol amount per unit area of gold is not relevant. Indeed, the furthest molecules from the gold surface in the channel during the injections under laminar flow have reduced chances to interact with this surface, hence questioning the relevance of the initial calculation.

		Test 1: 25.4 µM			**Test 2: 2.5 mM**			**Test 3: 25.4µM EtOH**			**Test 4: 1.3 µM**		
Flow channel	MA	Signal at 100s	% of signal at end injection	Signal balance	Signal at 100s	% of signal at end injection	Signal balance	Signal at 100s	% of signal at end injection	Signal balance	Signal at 100s	% of signal at end injection	Signal balance
FC1	TA	521	65	708	922	89	576	3980	84	679	392	39	568
FC2	MHA	737	73	657	445	81	237	4468	90 (but RI)	629	637	58	595

Table 2. Signal balance obtained for the different experimental conditions

As a conclusion, the best conditions among the tested ones for a rapid thiol monolayer self-assembling on the gold surface is obtained by injection of a thiol solution at 25.4 µM in water as a solvent.

Verification on the batch system

SPR experiments enable to compare the signal balance of the thiols grafting on a flat gold surface in different conditions, and the associated kinetics profile. It is now interesting to compare these results with those obtained for the thiols grafting on GNPs in the same conditions (25.4 µM and 2.5 mM of MA and 25.4µM in ethanol 10% (v/v)).

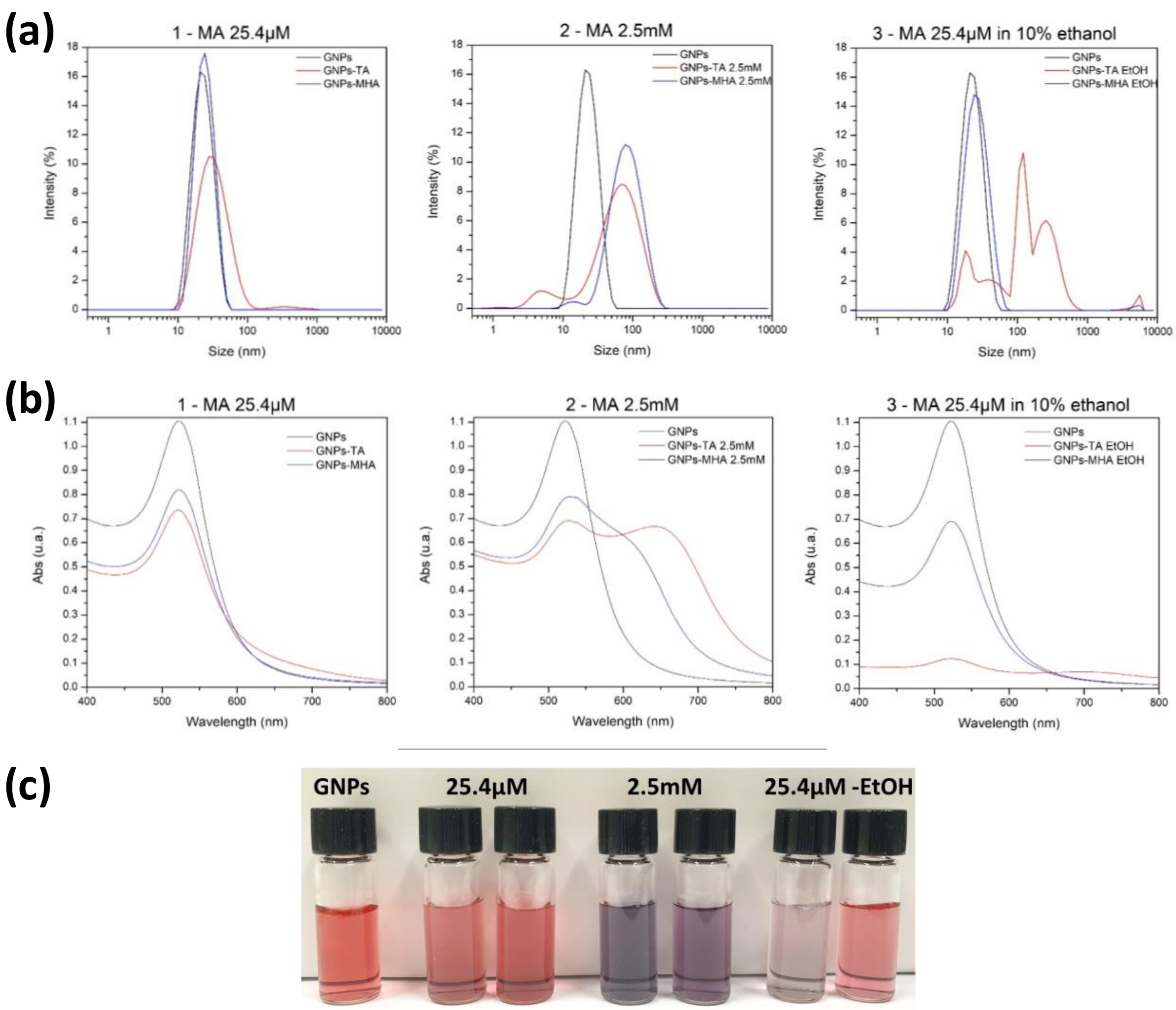

Figure 7: (a) Size distribution of the suspensions obtained by DLS by intensity (b) UV-visible spectra of the GNPs suspensions and (c) photograph of the GNPs suspensions (TA sample on the left and MHA on the right) obtained after washing in the different grafting conditions (1 - MA 25.4 µM, 2 - MA 2.5 mM, and 3 - MA 25.4 µM in 10% ethanol)

First, the size distribution in Figure 7-a allows to conclude on the dispersity of the obtained suspensions for the different conditions. With the 25.4 µM MA concentration, monodisperse suspensions are obtained except for a very small aggregated population for GNPs-TA with sizes of the same magnitude as in the initial GNPs suspension. At higher concentration, polydisperse suspensions are obtained with mainly two populations: an aggregated population with a significant size increase and a smaller population of individual particles. When the thiol suspension is added at this high concentration, a pH decrease of 1 to 2 units occurs, probably leading to GNPs destabilization even before the thiol derivatives can attach (Table S1 for the suspension pH after MA injection). When grafting is achieved with the initial 25.4 µM concentration but in the presence of ethanol, a polydisperse suspension is obtained for TA functionalized particles while monodispersity is preserved for MHA functionalized particles. Those conclusions can also be verified on Figure 7-b with the corresponding LSPR profiles that change as a consequence of aggregation. A broad peak is observed for the GNPs and the suspension grafted by TA and MHA at 25.4 µM with a maximum from 522 to 523 nm depending on the surrounding molecule. When the grafting concentration increases at 2.5 mM, Figure 7-b-2 shows a maximum at the same value, but another broad peak is observable near 660 nm for GNPs-TA and 630 nm for GNPs-MHA due to aggregation with sizes around 100 nm according to DLS. These additional broad peaks result in a color change from reddish pink to purple as shown in Figure 7-c. When the grafting is achieved in ethanol, the UV-Visible spectra in Figure 7-b-3 present a monodisperse suspension profile for

GNPs-MHA which confirms the DLS observation. However, the intensity is lower for the maximum LSPR peak for the suspension at 25.4 µM in ethanol (Abs = 0.691 corresponding to 0.158 mM of GNPs) than in water (Abs = 0.819 corresponding to 0.188 mM of GNPs) which indicates a lower yield in that case. For the GNPs-TA suspension, the presence of multiple populations in DLS is confirmed by the additional broad peak in the UV-Vis spectra around 700 nm. In addition, the very low absorption maximum at 0.124 indicates a low NPs recuperation rate after washing, which results in the increased translucent character of the suspension in Figure 7-c. Thus, the best conditions to obtain a monodisperse suspension of GNPs and the highest yields of functionalization by thiols is to add thiols at a concentration of 25.4µM in water. This result agrees with the conclusion reached with the SPR measurements.

Discussion

Same conclusion is obtained regarding the grafting efficiency of MA in different conditions when using both the SPR analysis and the classical characterization of batch GNPs suspensions.

In the end, higher grafting rates should ensure a better stability for the NPs suspension, limiting potential aggregation during the washing step by centrifugation, thus leading to better suspension monodispersity and nanoparticles recovery. This means that results obtained by SPR should generally be a good indication of the results obtained when grafting is achieved on batch suspensions.

However, some parameters are not taken into account or differ when using SPR. Indeed, flow circulation ensures continuous thiol derivatives supply, which is not the case on batch system where the media is depopulated of its molecules when they are adsorbed on the nanoparticles surface. Moreover, the washing method is different between the two systems with centrifugationredispersion of batches and flushing of a concentrated nonionic surfactant solution in SPR. Centrifugation in SPR is not possible and a simple water flushing may not be sufficient to eliminate adsorption. Using OG in GNPs batches probably would lead to aggregation and should anyway be removed at the end, so identical washing for the two systems cannot be implemented. Also, the NPs curvature cannot be taken into account on the chip and steric repulsion might be higher between molecules terminal groups and could eventually limit the final grafting density. Finally, the flow dynamics strongly differs between the two systems with a fixed flow rate in SPR and stirring for the batch system. Therefore, it is necessary to be careful during the comparison. Yet, even though the systems differ, the tendency obtained by SPR experiments are gathered in the same conditions, whether they differ from the batch system or not, so the comparison of the grafting conditions are still valid.

When studying grafting efficiency on gold nanoparticles suspension, the repetition of experiments implies to pledge some materials and products that can be expensive, and which are wasted in the case of aggregation, leading to waste and pollution that should be avoided [57-58]. Also, it takes a lot of time to perform the GNPs synthesis, the different grafting experiments, washings, and subsequent characterization. On the contrary, one only needs to check the weight balance on different flow paths after injection during SPR experiments. This is an additional advantage of the use of SPR to predict reactivity of thiol molecules on the gold nanoparticles. Finally, using SPR enables to easily obtain information on the grafting kinetics, which can be done by UV-visible spectroscopy for batch systems but with a low sensitivity for small molecules. Using SPR enables at least to rule out conditions leading to poor grafting, and in the best case to define the optimum grafting conditions before applications on larger batch quantities; then all the characterizations techniques can be implemented.

Conclusions

The grafting of two thiol derivatives (TA and MHA) on a gold surface in different conditions was studied by two different methods. On the one hand, SPR analysis of injection of thiol solutions on a naked gold chip was employed to monitor the kinetics and grafting rates. On the other hand, classical batch grafting was achieved by mixing thiols and GNPs in suspension and subsequent characterizations were made (TEM, UV-visible spectroscopy, DLS, Raman spectroscopy). Once combined, those characterizations bring information on grafting success, suspension final quality in terms of stability and dispersion state and nanoparticles yields. Both methods identify the best grafting conditions to employ to get higher grafting rates in the chip case, and higher NPs yield and best stability and monodispersity in the batch case. We reached the same conclusion with both methods, namely that in our conditions the lower thiol concentration provided the best grafting conditions.

Even though a few differences can be pointed out when using SPR system as a comparison with nanoparticles suspension (curvature radius, flow circulation versus closed system, washing), the SPR method offers several advantages. Indeed, the grafting efficiency upon different conditions can be compared directly during the experiments when many complementary analyses have to be carried out on GNPs suspensions. It also prevents materials waste, and allows easy access to the reaction kinetics whose study is more difficult to implement for GNPs suspensions.

This study provides a new method for the selection of functionalization parameters to use when grafting thiol molecules on gold nanoparticles. This method can be applied to other thiol derivatives and other grafting conditions as long as they are compatible with the SPR device. Finally, the method can also be applied to other metallic surfaces as long as they have a surface plasmon resonance (silver [55, 59], aluminum [60-61]…) and to very thin non-plasmonic layers (silica, glass-like…)[62] deposited on a plasmonic chip. In that case, different ligand chemical functions can be used such as thiols for silver, phosphonates for aluminum, and others for silica and glass-like decorated materials.

ASSOCIATED CONTENT

Supporting Information. Additional information, results and characterization details including molecules formulas, TEM distribution, UV-visible spectroscopy of aged samples, and SPR experiment results.

Supporting information files are available free of charge.

AUTHOR INFORMATION

Corresponding Author

* Wilfrid Boireau – Université de Franche-Comté, CNRS, institut FEMTO-ST, 15B Avenue des Montboucons, F-25030 Besançon, France – Email wilfrid.boireau@femto-st.fr

* Nadine Millot - Laboratoire Interdisciplinaire Carnot de Bourgogne, UMR 6303 CNRS/Université de Bourgogne, 9 Avenue Alain Savary, BP 47870, Dijon, 21078 France – Email Nadine.Millot@u-bourgogne.fr

ACKNOWLEDGMENT

This work was supported by the EIPHI Graduate School (contract ANR-17-EURE-0002).

The authors wish to thank the clean room and characterization laboratory staff at MIMENTO platform, FEMTO-Engineering and at the Clinical-Innovation Proteomic Platform (CLIPP).

Authors also gratefully thank Dr. R. Chassagnon for TEM experiments.

REFERENCES

1. Dreaden, E. C.; Alkilany, A. M.; Huang, X.; Murphy, C. J.; El-Sayed, M. A., The Golden Age: Gold Nanoparticles for Biomedicine. *Chemical Society Reviews* **2012**, *41*, 2740-2779.

2. Jeong, H.-H.; Choi, E.; Ellis, E.; Lee, T.-C., Recent Advances in Gold Nanoparticles for Biomedical Applications: From Hybrid Structures to Multi-Functionality. *Journal of Materials Chemistry B* **2019**, *7*, 3480-3496.

3. Mejía-Salazar, J. R.; Oliveira, O. N., Jr., Plasmonic Biosensing. *Chemical Reviews* **2018**, *118*, 10617-10625.

4. Gelle, A.; Moores, A., Plasmonic Nanoparticles: Photocatalysts with a Bright Future. *CURRENT OPINION IN GREEN AND SUSTAINABLE CHEMISTRY* **2019**, *15*, 60-66.

5. Qi, M.; Zhang, N. M. Y.; Li, K. W.; Tjin, S. C.; Wei, L., Hybrid Plasmonic Fiber-Optic Sensors. *SENSORS* **2020**, *20*, 3266.

6. Olaimat, M. M.; Yousefi, L.; Ramahi, O. M., Using Plasmonics and Nanoparticles to Enhance the Efficiency of Solar Cells: Review of Latest Technologies. *J. Opt. Soc. Am. B* **2021**, *38*, 638-651.

7. Amendola, V.; Pilot, R.; Frasconi, M.; Maragò, O. M.; Iatì, M. A., Surface Plasmon Resonance in Gold Nanoparticles: A Review. *Journal of Physics: Condensed Matter* **2017**, *29*, 203002.

8. Giljohann, D. A.; Seferos, D. S.; Daniel, W. L.; Massich, M. D.; Patel, P. C.; Mirkin, C. A., Gold Nanoparticles for Biology and Medicine. *Angewandte Chemie International Edition* **2010**, *49*, 3280-3294.

9. Wu, Y.; Ali, M. R. K.; Chen, K.; Fang, N.; El-Sayed, M. A., Gold Nanoparticles in Biological Optical Imaging. *Nano Today* **2019**, *24*, 120-140.

10. Loh, X. J.; Lee, T.-C.; Dou, Q.; Deen, G. R., Utilising Inorganic Nanocarriers for Gene Delivery. *Biomaterials Science* **2016**, *4*, 70-86.

11. Bilynsky, C.; Millot, N.; Papa, A.-L., Radiation Nanosensitizers in Cancer Therapy—from Preclinical Discoveries to the Outcomes of Early Clinical Trials. *Bioengineering & Translational Medicine* **2022**, *7*, e10256.

12. Schuemann, J., et al., Roadmap for Metal Nanoparticles in Radiation Therapy: Current Status, Translational Challenges, and Future Directions. *Physics in Medicine & Biology* **2020**, *65*, 21RM02.

13. Vines, J. B.; Yoon, J.-H.; Ryu, N.-E.; Lim, D.-J.; Park, H., Gold Nanoparticles for Photothermal Cancer Therapy. *Frontiers in Chemistry* **2019**, *7*, 1-16.

14. Biju, V., Chemical Modifications and Bioconjugate Reactions of Nanomaterials for Sensing, Imaging, Drug Delivery and Therapy. *Chemical Society Reviews* **2014**, *43*, 744-764.

15. Sperling, R. A.; Parak, W. J., Surface Modification, Functionalization and Bioconjugation of Colloidal Inorganic Nanoparticles. *Philosophical Transactions of the Royal Society A: Mathematical, Physical and Engineering Sciences* **2010**, *368*, 1333-1383.

16. Thanh, N. T. K.; Green, L. A. W., Functionalisation of Nanoparticles for Biomedical Applications. *Nano Today* **2010**, *5*, 213-230.

17. Turkevich, J.; Stevenson, P. C.; Hillier, J., A Study of the Nucleation and Growth Processes in the Synthesis of Colloidal Gold. *Discussions of the Faraday Society* **1951**, *11*, 55-75.

18. Kimling, J.; Maier, M.; Okenve, B.; Kotaidis, V.; Ballot, H.; Plech, A., Turkevich Method for Gold Nanoparticle Synthesis Revisited. *The Journal of Physical Chemistry B* **2006**, *110*, 15700-15707.

19. Frens, G., Controlled Nucleation for the Regulation of the Particle Size in Monodisperse Gold Suspensions. *Nature Physical Science* **1973**, *241*, 20-22.

20. Park, J.-W.; Shumaker-Parry, J. S., Structural Study of Citrate Layers on Gold Nanoparticles: Role of Intermolecular Interactions in Stabilizing Nanoparticles. *Journal of the American Chemical Society* **2014**, *136*, 1907-1921.

21. Grys, D.-B.; de Nijs, B.; Salmon, A. R.; Huang, J.; Wang, W.; Chen, W.-H.; Scherman, O. A.; Baumberg, J. J., Citrate Coordination and Bridging of Gold Nanoparticles: The Role of Gold Adatoms in Aunp Aging. *ACS Nano* **2020**, *14*, 8689-8696.

22. Kolb, A. N. D.; Johnston, J. H., Synthesis and Functionalisation of Stable 'Naked' Gold Nanoparticles. *International Journal of Nanotechnology* **2017**, *14*, 179-190.

23. Giersig, M.; Mulvaney, P., Preparation of Ordered Colloid Monolayers by Electrophoretic Deposition. *Langmuir* **1993**, *9*, 3408-3413.

24. Templeton, A. C.; Wuelfing, W. P.; Murray, R. W., Monolayer-Protected Cluster Molecules. *Accounts of Chemical Research* **2000**, *33*, 27-36.

25. Bard, A.; Rondon, R.; Marquez, D. T.; Lanterna, A. E.; Scaiano, J. C., How Fast Can Thiols Bind to the Gold Nanoparticle Surface? *Photochemistry and Photobiology* **2018**, *94*, 1109-1115.

26. Locardi, F.; Canepa, E.; Villa, S.; Nelli, I.; Lambruschini, C.; Ferretti, M.; Canepa, F., Thermogravimetry and Evolved Gas Analysis for the Investigation of Ligand-Exchange Reaction in Thiol-Functionalized Gold Nanoparticles. *Journal of Analytical and Applied Pyrolysis* **2018**, *132*, 11-18.

27. Bajaj, M.; Wangoo, N.; Jain, D. V. S.; Sharma, R. K., Quantification of Adsorbed and Dangling Citrate Ions on Gold Nanoparticle Surface Using Thermogravimetric Analysis. *Scientific Reports* **2020**, *10*, 8213.

28. Techane, S. D.; Gamble, L. J.; Castner, D. G., X-Ray Photoelectron Spectroscopy Characterization of Gold Nanoparticles Functionalized with Amine-Terminated Alkanethiols. *Biointerphases* **2011**, *6*, 98.

29. Wang, Y.; Zeiri, O.; Neyman, A.; Stellacci, F.; Weinstock, I. A., Nucleation and Island Growth of Alkanethiolate Ligand Domains on Gold Nanoparticles. *ACS Nano* **2012**, *6*, 629-640.

30. Englebienne, P.; Van Hoonacker, A.; Verhas, M., High-Throughput Screening Using the Surface Plasmon Resonance Effect of Colloidal Gold Nanoparticles. *Analyst* **2001**, *126*, 1645-1651.

31. Dileseigres, A. S.; Prado, Y.; Pluchery, O., How to Use Localized Surface Plasmon for Monitoring the Adsorption of Thiol Molecules on Gold Nanoparticles? *Nanomaterials* **2022**, *12*, 292.

32. Kravets, V. G.; Kabashin, A. V.; Barnes, W. L.; Grigorenko, A. N., Plasmonic Surface Lattice Resonances: A Review of Properties and Applications. *Chemical Reviews* **2018**, *118*, 5912-5951.

33. Haiss, W.; Thanh, N. T. K.; Aveyard, J.; Fernig, D. G., Determination of Size and Concentration of Gold Nanoparticles from Uv−Vis Spectra. *Analytical Chemistry* **2007**, *79*, 4215-4221.

34. Miller, M. M.; Lazarides, A. A., Sensitivity of Metal Nanoparticle Surface Plasmon Resonance to the Dielectric Environment. *The Journal of Physical Chemistry B* **2005**, *109*, 21556-21565.

35. Mondal, B.; Zeng, S., Recent Advances in Surface Plasmon Resonance for Biosensing Applications and Future Prospects. In *Nanophotonics in Biomedical Engineering*, Springer, Singapore: 2020; pp 21-48.

36. Duan, Q.; Liu, Y.; Chang, S.; Chen, H.; Chen, J.-h. Surface Plasmonic Sensors: Sensing Mechanism and Recent Applications *Sensors* **2021**, DOI: 10.3390/s21165262.

37. Hamza, M. E.; Othman, M. A.; Swillam, M. A. Plasmonic Biosensors: Review *Biology* **2022**, DOI: 10.3390/biology11050621.

38. Mansuy-Schlick, V.; Delage-Mourroux, R.; Jouvenot, M.; Boireau, W., Strategy of Macromolecular Grafting onto a Gold Substrate Dedicated to Protein-Protein Interaction Measurements. *Biosens Bioelectron* **2006**, *21*, 1830-7.

39. Myszka, D. G., Kinetic Analysis of Macromolecular Interactions Using Surface Plasmon Resonance Biosensors. *Current Opinion in Biotechnology* **1997**, *8*, 50-57.

40. Zhou, X.; Chen, K.; Li, L.; Peng, W.; Yu, Q., Angle Modulated Surface Plasmon Resonance Spectrometer for Refractive Index Sensing with Enhanced Detection Resolution. *Optics Communications* **2017**, *382*, 610-614.

41. Englebienne, P.; Van Hoonacker, A.; Verhas, M., Surface Plasmon Resonance: Principles, Methods and Applications in Biomedical Sciences. *SPECTROSCOPY-AN INTERNATIONAL JOURNAL* **2003**, *17*, 255-273.

42. Tawil, N.; Hatef, A.; Sacher, E.; Maisonneuve, M.; Gervais, T.; Mandeville, R.; Meunier, M., Surface Plasmon Resonance Determination of the Binding Mechanisms of L-Cysteine and Mercaptoundecanoic Acid on Gold. *The Journal of Physical Chemistry C* **2013**, *117*, 6712-6718.

43. Damos, F. S.; Luz, R. C. S.; Kubota, L. T., Determination of Thickness, Dielectric Constant of Thiol Films, and Kinetics of Adsorption Using Surface Plasmon Resonance. *Langmuir* **2005**, *21*, 602-609.

44. Debono, R. F.; Loucks, G. D.; Manna, D. D.; Krull, U. J., Self-Assembly of Short and Long-Chain N-Alkyl Thiols onto Gold Surfaces: A Real-Time Study Using Surface Plasmon Resonance Techniques. *Canadian Journal of Chemistry* **1996**, *74*, 677-688.

45. Villarreal, E.; Li, G. G.; Zhang, Q.; Fu, X.; Wang, H., Nanoscale Surface Curvature Effects on Ligand–Nanoparticle Interactions: A Plasmon-Enhanced Spectroscopic Study of Thiolated Ligand Adsorption, Desorption, and Exchange on Gold Nanoparticles. *Nano Letters* **2017**, *17*, 4443-4452.

46. Elie-Caille, C.; Rauch, J.-Y.; Rouleau, A.; Boireau, W., Preparation of Flat Gold Terraces for Protein Chip Developments. *Micro and Nano Letters* **2009**, *4*, 88-94.

47. *Biacore 3000 Instrument Handbook*, Edition AG ed.; GE Healthcare, 2007; Vol. BR-1003-81, p 346.

48. Mabuchi, M.; Takenaka, T.; Fujiyoshi, Y.; Uyeda, N., Surface Enhanced Raman Scattering of Citrate Ions Adsorbed on Gold Sol Particles. *Surface Science* **1982**, *119*, 150-158.

49. Zhou, J.-G.; Williams, Q. L.; Wu, R., Thioglycolic Acid on the Gold (111) Surface and Raman Vibrational Spectra. *The Journal of Chemical Physics* **2010**, *132*, 064702.

50. Królikowska, A.; Kudelski, A.; Michota, A.; Bukowska, J., Sers Studies on the Structure of Thioglycolic Acid Monolayers on Silver and Gold. *Surface Science* **2003**, *532-535*, 227-232.

51. Silveira, R. L.; Mamián-López, M. B.; Rubim, J. C.; Temperini, M. L. A.; Corio, P.; Santos, J. J., Spectroscopic and Electrophoresis Study of Substitution on the Surface of Gold Nanoparticles by Different Mercaptoalkyl Carboxylic Acids and Bioconjugation with Bovine Serum Albumin. *Analytical and Bioanalytical Chemistry* **2019**, *411*, 3047-3058.

52. Stenberg, E.; Persson, B.; Roos, H.; Urbaniczky, C., Quantitative Determination of Surface Concentration of Protein with Surface Plasmon Resonance Using Radiolabeled Proteins. *Journal of Colloid and Interface Science* **1991**, *143*, 513-526.

53. Jung, L. S.; Campbell, C. T.; Chinowsky, T. M.; Mar, M. N.; Yee, S. S., Quantitative Interpretation of the Response of Surface Plasmon Resonance Sensors to Adsorbed Films. *Langmuir* **1998**, *14*, 5636-5648.

54. Ghorai, P. K.; Glotzer, S. C., Molecular Dynamics Simulation Study of Self-Assembled Monolayers of Alkanethiol Surfactants on Spherical Gold Nanoparticles. *The Journal of Physical Chemistry C* **2007**, *111*, 15857-15862.

55. Love, J. C.; Estroff, L. A.; Kriebel, J. K.; Nuzzo, R. G.; Whitesides, G. M., Self-Assembled Monolayers of Thiolates on Metals as a Form of Nanotechnology. *Chemical Reviews* **2005**, *105*, 1103-1170.

56. Xue, Y.; Li, X.; Li, H.; Zhang, W., Quantifying Thiol–Gold Interactions Towards the Efficient Strength Control. *Nature Communications* **2014**, *5*, 4348.

57. OECD, *Nanomaterials in Waste Streams : Current Knowledge on Risks and Impacts*; OECD Publishing, Paris, 2016, p 96 pages.

58. Musee, N., Nanowastes and the Environment: Potential New Waste Management Paradigm. *Environment International* **2011**, *37*, 112-128.

59. Wang, G.; Wang, C.; Yang, R.; Liu, W.; Sun, S. A Sensitive and Stable Surface Plasmon Resonance Sensor Based on Monolayer Protected Silver Film *Sensors* **2017**, DOI: 10.3390/s17122777.

60. Liu, Q.; Ma, Z.; Wu, Q.; Wang, W., The Biochemical Sensor Based on Liquid-Core Photonic Crystal Fiber Filled with Gold, Silver and Aluminum. *Optics & Laser Technology* **2020**, *130*, 106363.

61. Tambe, N. S.; Bhushan, B., Nanotribological Characterization of Self-Assembled Monolayers Deposited on Silicon and Aluminium Substrates. *Nanotechnology* **2005**, *16*, 1549.

62. Herth, E.; Zeggari, R.; Rauch, J.-Y.; Remy-Martin, F.; Boireau, W., Investigation of Amorphous Siox Layer on Gold Surface for Surface Plasmon Resonance Measurements. *Microelectronic Engineering* **2016**, *163*, 43-48.

TOC Graphic